Supplemental Information

Ca^{2+}-activated K^+ channels reduce network excitability, improving adaptability and energetics for transmitting and perceiving sensory information

Xiaofeng Li, Ahmad Abou Tayoun, Zhuoyi Song, An Dau, Diana Rien, David Jaciuch, Sidhartha Dongre, Florence Blanchard, Anton Nikolaev, Lei Zheng, Murali K. Bollepalli, Brian Chu, Roger C. Hardie, Patrick J. Dolph and Mikko Juusola

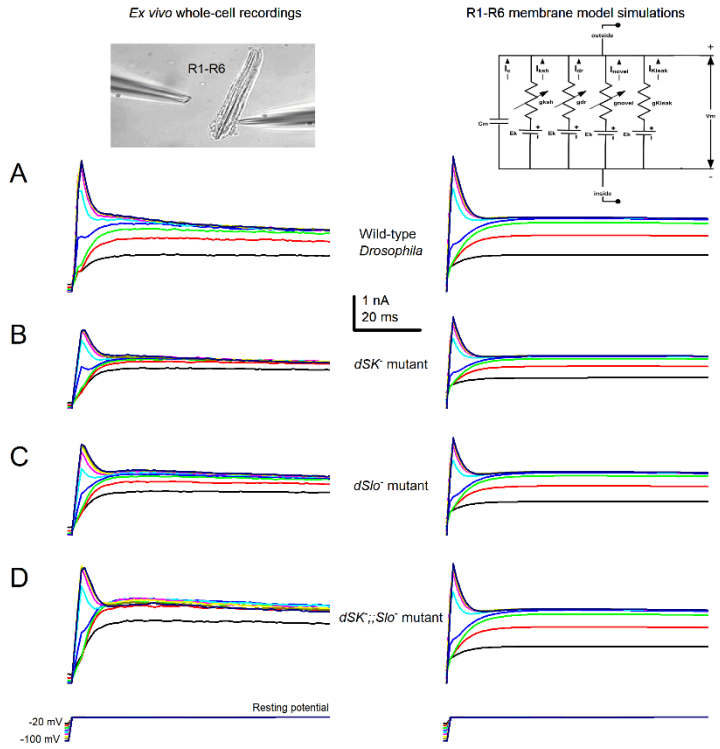

Figure S1, related to Figures 3, 5, S2 and S3. Characteristic voltage-sensitive *shaker* and *shab* K^+ current responses of (A) wild-type, (B) *dSK*$^-$, (C) *dSlo*$^-$ and (D) *dSK*$^-$*;;dSlo*$^-$ R1-R6 photoreceptors and their HH-models to voltage commands, under whole-cell voltage-clamp conditions.

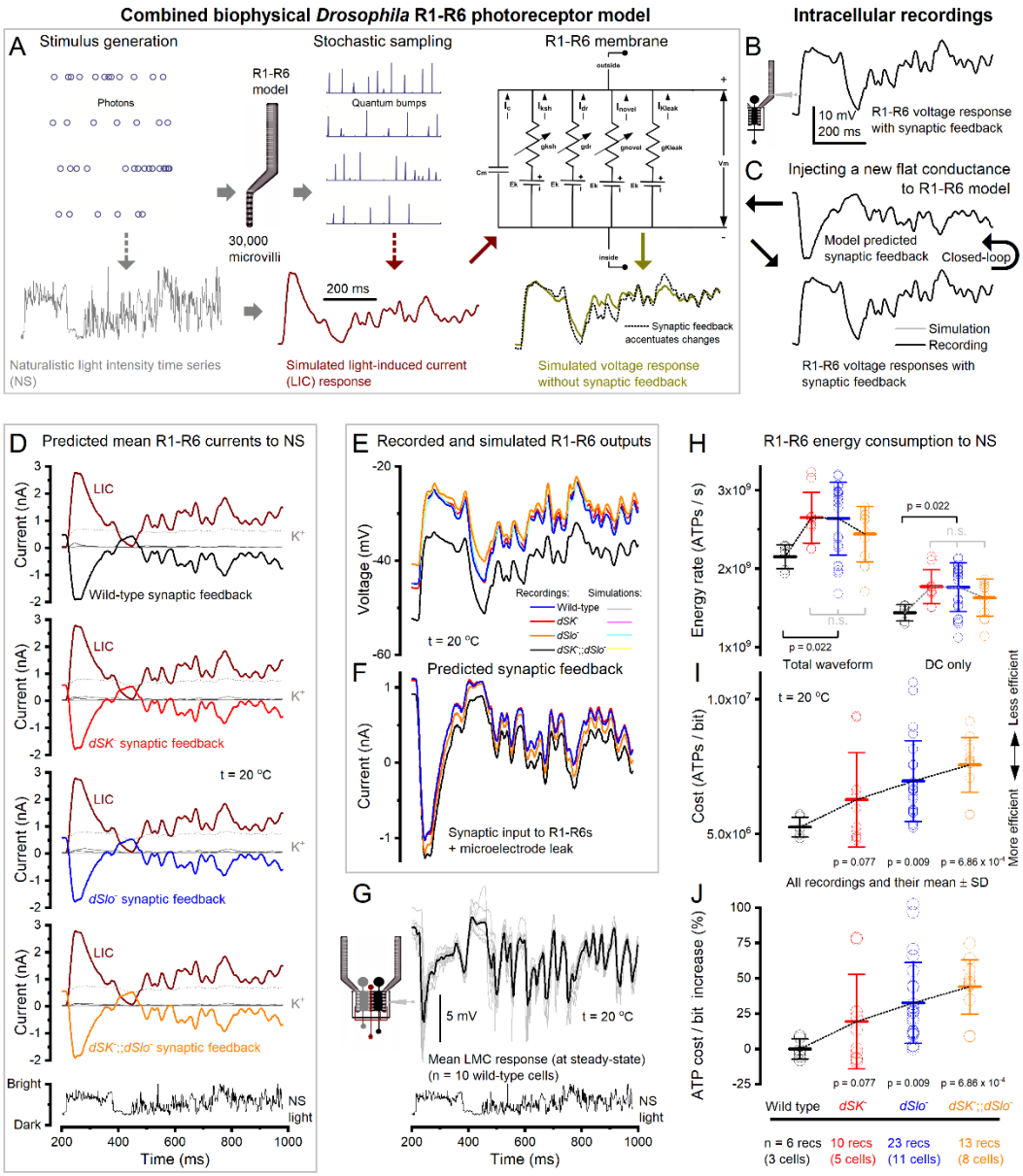

Figure S2, related to Figures 5 and S3. Examples of the wild-type (black), *dSK*⁻ (red), *dSlo*⁻ (blue) and *dSK*⁻;;*dSlo*⁻ (orange data) photoreceptor models' *shaker*, *shab*, K^+-leak, LIC and synaptic feedback currents to naturalistic light stimulation, when using the same wild-type *shaker* and *shab* conductance dynamics in all the models.

(A) In these simulations, the while-type, *dSK*⁻, *dSlo*⁻ and *dSK*⁻;;*dSlo*⁻ R1-R6 models had identical light induced current (LIC) and voltage-sensitive membrane conductances (the models used the wild-type shaker and shab dynamics as in Figure S1A; cf. Figure 5A).

(B) Characteristic recording waveform to bright NS (BG0).

(C) Again, synaptic feedback was computed through the R1-R6 model, which had no free parameters, in a closed-loop until the model output (gray) matched the recorded output (black).

(D) The fixed light-induced (dark red), K^+ currents and the average predicted synaptic feedback of wild-type and mutant R1-R6 recordings.

(E) Together, these currents charged up their respective simulated R1-R6 voltage responses. The simulations (light colors) matched the recordings (bright colors).

(F) Again, the average predicted synaptic feedbacks to the mutant R1-R6s were stronger, having higher means (tonic excitatory background) than the wild-type.

(G) The recorded large monopolar cell (LMC) response waveforms to the same NS resembled the predicted feedback waveforms (in F).

(H) The ATP consumption of these mutant R1-R6 models was 3.5-8.6% higher than in those models, which had their recorded (smaller) *shaker* and *shab* conductances (cf. Figures 3F-H and 5H).
(I) The cost of neural information, was calculated for each recording by dividing its information rate estimate with its full ATP consumption rate estimate. On average, the absence of dSK or dSlo or both increased the cost of information in a mutant R1-R6 by 19.3 ± 33.4% (*dSK*$^{-}$), 32.6 ± 28.6% (*dSlo*$^{-}$) or 43.9 ± 19.3% (*dSK*$^{-}$;;*dSlo*$^{-}$). Thus, 19-36% homeostatic reductions in *shaker* and *shab* currents in *dSK*$^{-}$ and *dSlo*$^{-}$ R1-R6 photoreceptors caused only 4.5% and 6.2% savings in their ATP consumption per each bit of transmitted information (cf. Figures 5I and 5J).

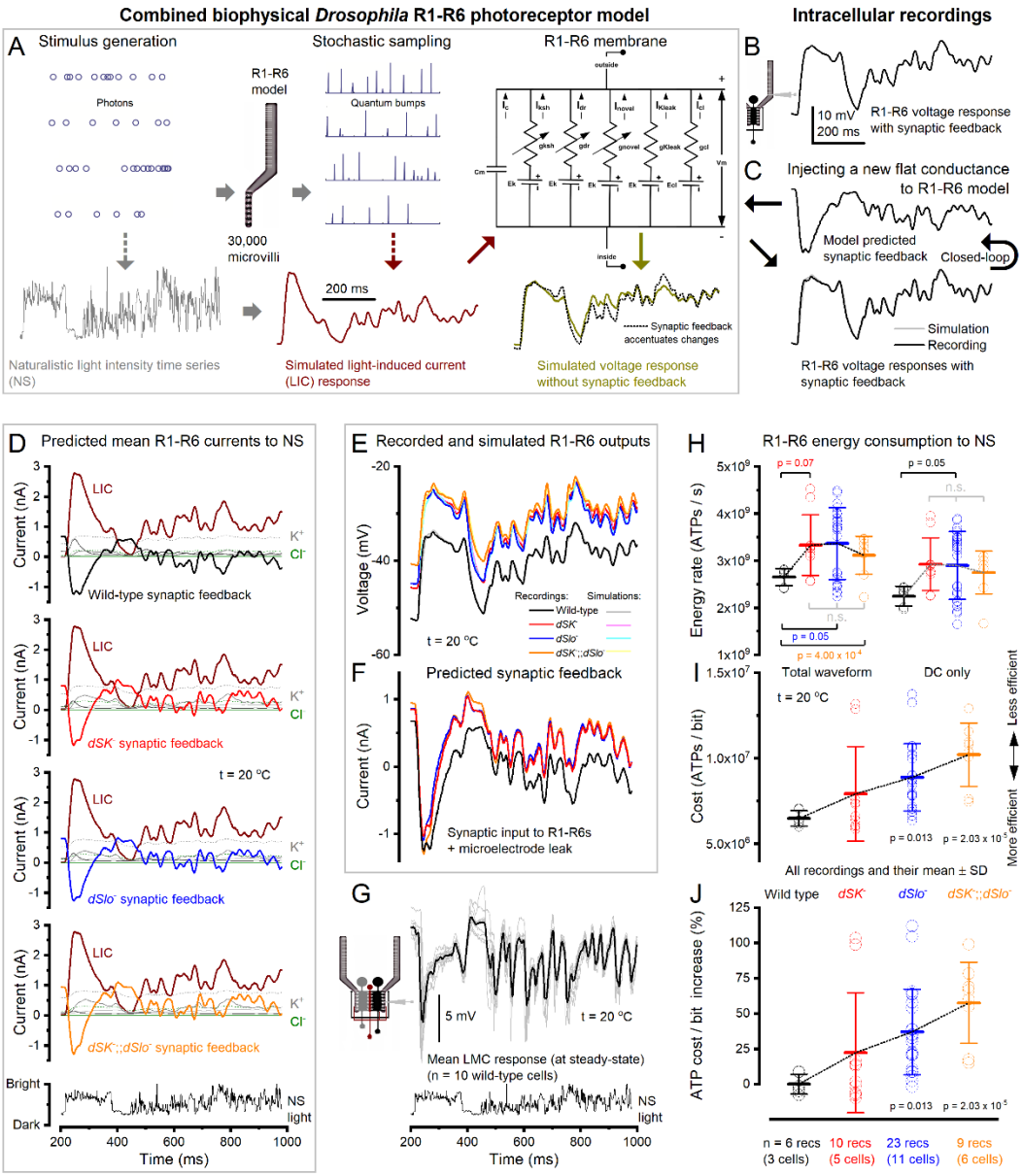

Figure S3, related to Figures 5 and S2. Examples of the wild-type (black), *dSK*⁻ (red), *dSlo*⁻ (blue) and *dSK*⁻*;;dSlo*⁻ (orange data) photoreceptor models' *shaker*, *shab*, K^+-leak, Cl^--leak LIC and synaptic feedback currents to naturalistic light stimulation, when using larger wild-type *shaker* and *shab* conductance dynamics (as in Table S2) in all the models.

(A) In these simulations, we further added a Cl^--leak and Cl^- conductance in the R1-R6 photoreceptor membrane model and balanced these by increasing voltage-sensitive K^+ conductances (STAR Methods: speculative photoreceptor membrane model), and again the synaptic feedback (Juusola et al., 2017a; Song and Juusola, 2017) was computed in a closed-loop until the simulations matched the recordings (cf. Figure 4C).
(B) Characteristic recording waveform to bright NS (BG0).
(C) Synaptic feedback to each recording was estimated computationally by linking it to the photoreceptor model, which had no free parameters.
(D) The fixed light-induced (dark red), K^+ and Cl^- currents and the average predicted synaptic feedback and of wild-type and mutant R1-R6 recordings.
(E) These currents charged up their respective simulated R1-R6 voltage responses (light colors), which matched the actual recordings (bright colors).

(F) Similar to the other simulations (cf. Figures 5E and S2E), the predicted synaptic feedback to the mutant R1-R6s was larger (carrying bigger modulation) with a higher mean (tonic excitatory background) than the wild-type. However, the modulation in these simulations was even more transient.
(G) Separately recorded large monopolar cell (LMC) response waveforms to the same NS much resemble the predicted feedback waveforms (in F).
(H) Energy (ATP) consumption of each recording was calculated for its full waveform (left) (Song and Juusola, 2014) and DC voltage (right) (Laughlin et al., 1998), respectively. Notably, the added extra Cl^--leak and Cl^- conductance (with rebalanced K^+ conductances) increased the photoreceptors' energy usage by ~26.3% (cf. Figure 5H, left: from 2.10 x 10^9 ATP/s to 2.65 x 10^9 ATP/s,). Whilst the original DC voltage method (right), which does not consider how the dynamic ion fluctuations add to the electrochemical pumping work, now underestimated ATP consumption by about 15%.
(I) The cost of neural information, was calculated for each recording by dividing its information rate estimate with its full ATP consumption rate estimate. Here, homeostatic increase in K^+ and Cl^- leak conductances (to compensate the loss of Ca^{2+}-activated K^+ channels) increased the cost of information in a mutant R1-R6 by 22.2 ± 42.3% (*dSK*$^-$), 37.0 ± 30.3% (*dSlo*$^-$) or 57.6 ± 28.8% (*dSK*$^-$;;*dSlo*$^-$), in respect to the comparable wild-type model.

Table S1, related to Figures 5 and S2. Conservative photoreceptor HH-membrane model parameters:

R1-R6 model	V_{rest}	C_m	$E_{Cl\text{-}leak}$	Cl^- leak	E_{K+}	K^+ leak	E_{LIC}	LIC leak	E_{Syn}	Syn leak	K_{Shab} max	K_{Shaker} max	K_{new} max
Wild-type	-65 mV	1 µF/cm^2	-57.1 mV	0	-85 mV	8.5 x10^{-4} S/cm^2	0	0	-5 mV	0	0.0024 S/cm^2	0.005 S/cm^2	1.1 x 10^{-4} S/cm^2
dSK$^-$	-65 mV	1 µF/cm^2	-57.1 mV	0	-85 mV	8.5 x10^{-4} S/cm^2	0	0	-5 mV	0	0.00144 S/cm^2	0.003 S/cm^2	1.1 x 10^{-4} S/cm^2
dSlo$^-$	-65 mV	1 µF/cm^2	-57.1 mV	0	-85 mV	8.5 x10^{-4} S/cm^2	0	0	-5 mV	0	0.00192 S/cm^2	0.00325 S/cm^2	1.1 x 10^{-4} S/cm^2
dSK$^-$;; *dSlo*$^-$	-65 mV	1 µF/cm^2	-57.1 mV	0	-85 mV	8.5 x10^{-4} S/cm^2	0	0	-5 mV	0	0.0024 S/cm^2	0.00425 S/cm^2	1.1 x 10^{-4} S/cm^2

Table S2, related to Figure S3. Speculative photoreceptor HH-membrane model parameters:

R1-R6 model	V_{rest}	C_m	$E_{Cl\text{-}leak}$	Cl^- leak	E_{K+}	K^+ leak	E_{LIC}	LIC leak	E_{Syn}	Syn leak	K_{Shab} max	K_{Shaker} max	K_{new} max
Wild-type	-65 mV	1 µF/cm^2	-57.1 mV	5.85 x10^{-4} S/cm^2	-85 mV	8.5 x10^{-4} S/cm^2	0	0	-5 mV	0	0.009 S/cm^2	0.02 S/cm^2	0.001 S/cm^2
dSK$^-$	-65 mV	1 µF/cm^2	-57.1 mV	5.85 x10^{-4} S/cm^2	-85 mV	8.5 x10^{-4} S/cm^2	0	0	-5 mV	0	0.009 S/cm^2	0.01 S/cm^2	0.001 S/cm^2
dSlo$^-$	-65 mV	1 µF/cm^2	-57.1 mV	5.85 x10^{-4} S/cm^2	-85 mV	8.5 x10^{-4} S/cm^2	0	0	-5 mV	0	0.009 S/cm^2	0.02 S/cm^2	0.001 S/cm^2
dSK$^-$;; *dSlo*$^-$	-65 mV	1 µF/cm^2	-57.1 mV	5.85 x10^{-4} S/cm^2	-85 mV	8.5 x10^{-4} S/cm^2	0	0	-5 mV	0	0.009 S/cm^2	0.02 S/cm^2	0.001 S/cm^2